



# Development of lead free pulse electrodeposited tin based composite solder coating reinforced with ex situ cerium oxide nanoparticles



Ashutosh Sharma<sup>a,\*</sup>, Sumit Bhattacharya<sup>a</sup>, Siddhartha Das<sup>a</sup>, H.-J. Fecht<sup>b</sup>, Karabi Das<sup>a</sup>

<sup>a</sup> Department of Metallurgical and Materials Engineering, Indian Institute of Technology Kharagpur, Kharagpur 721 302, India

<sup>b</sup> Institut für Mikro- und Nanomaterialien, Universität Ulm, D-89081 Ulm, Germany

## ARTICLE INFO

### Article history:

Received 7 May 2013

Accepted 4 June 2013

Available online 14 June 2013

### Keywords:

Composites

Chemical synthesis

Electrochemical reactions

Microstructure

## ABSTRACT

Pure Sn and Sn–CeO<sub>2</sub> nanocomposite films have been pulse electrodeposited from an aqueous electrolyte containing stannous chloride (SnCl<sub>2</sub>·2H<sub>2</sub>O) and triammonium citrate (C<sub>6</sub>H<sub>17</sub>N<sub>3</sub>O<sub>7</sub>). The codeposition is achieved by adding different amounts of ball milled CeO<sub>2</sub> nanopowders (1–30 g/L) with a mean particle size of ~30 nm to the electrolyte. Microstructural characterizations have been carried out by X-ray diffraction analysis, scanning electron microscopy coupled with an energy dispersive spectroscopy, and transmission electron microscopy. The microstructural observations show that a uniform microstructure is obtained at a concentration of ~6 wt% CeO<sub>2</sub> in the deposits corresponding to 15 g/L CeO<sub>2</sub> in electrolyte. Thus, incorporation of an optimum amount of CeO<sub>2</sub> in a composite provides better mechanical, and wear and friction properties, without sacrificing the electrical resistivity significantly.

© 2013 Elsevier B.V. All rights reserved.

## 1. Introduction

Soldering materials are the backbone of various microelectronic devices and circuits that provide good electrical continuity, and thermal and mechanical strength to the electrical joints. They join the various integrated circuits (IC) to the base substrate. In addition, their presence assist in heat endurance and mechanical grip to hold the electric components on the Integrated circuits (IC) and printed circuit boards (PCB) [1,2]. In the past, various tin-lead alloys have been synthesized for packaging applications. However, in recent scenario there is a ban on the usage of electronic devices containing toxic lead and other hazardous wastes [3]. Therefore, the electronic manufacturers are now looking for lead free alternatives. Many studies have been carried out in the past to find out the alternatives for Sn–Pb solders. Lead free alloys such as pure tin (Sn), tin–silver (Sn–Ag), tin–bismuth (Sn–Bi), tin–copper (Sn–Cu) etc. are being developed and studied [1–4]. However, their strength is poor. Therefore, not only lead free but superior strength solders are required to make sure the electrical performance of an electronic device. An attractive way to strengthen the solder joint efficiently is to use a composite solder where reinforcements are added into a solder alloy [5–8]. The presence of the second phase (such as ceramic reinforcements) has been proposed as the better mechanism for controlling the reliability of the solder joints over monolithic solder. In literature, powder metallurgy route has been

often used to fabricate the lead-free solders reinforced with Al<sub>2</sub>O<sub>3</sub>, SnO<sub>2</sub>, SiC, TiB<sub>2</sub>, Si<sub>3</sub>N<sub>4</sub>, ZrO<sub>2</sub>, and Y<sub>2</sub>O<sub>3</sub> [5–6,9–13]. The presence of the secondary phases has been shown to refine the intermetallic compounds that enhance the reliability of the solder joints. Recently, Choi et al. [14] reinforced Sn matrix with carbon nanotubes by an electrodeposition process. However, there is limited research on the synthesis of electrodeposited lead free nanocomposite solders.

In the current research, CeO<sub>2</sub> particulates at the nanometre length scale have been used as reinforcement. In spite of attractive mechanical, thermal and electrical properties, CeO<sub>2</sub> has been rarely selected to reinforce Sn based solders. The main advantages of CeO<sub>2</sub> are (a) higher solution conductivity as compared to zirconia, (b) good corrosion resistance, and (c) resistance to oxidation [15]. In this study, composite solders reinforced with nanosized CeO<sub>2</sub> particulates have been synthesized using the pulse co-electrodeposition technique. Monolithic and composite solders have been characterized in terms of microstructure, mechanical, physical, wear, and electrical properties.

## 2. Experimental procedure

### 2.1. Pulse co-electrodeposition

The tin plating bath used for the electrodeposition consists of SnCl<sub>2</sub>·2H<sub>2</sub>O (50 g/L) and C<sub>6</sub>H<sub>17</sub>N<sub>3</sub>O<sub>7</sub> (100 g/L). The bath compositions and the electrical parameters are given in Table 1. The reinforcement CeO<sub>2</sub> nanoparticles are produced by high energy ball milling of as received CeO<sub>2</sub> powder (Loba Chemie, 99.8%) for 20 h in a Fritsch Pulverisette-6 vario planetary mill, Germany. The process control used is toluene with a ball to powder weight ratio of 10:1.

\* Corresponding author. Tel.: +91 9868054950/9832729427; fax: +91 (03222) 220 666/255 303.

E-mail address: [stannum.ashu@gmail.com](mailto:stannum.ashu@gmail.com) (A. Sharma).

**Table 1**  
Bath compositions and operating parameters.

Experimental parameters	Values
SnCl <sub>2</sub> ·2H <sub>2</sub> O	50 g/L
Triton X-100	0.1 g/L
Nanosized CeO <sub>2</sub>	0–30 g/L
pH	4.3
Current density	0.2 A/cm <sup>2</sup>
Bath temperature	28 °C
Duration	10 min
Anode	(99.8%) tin plate
Agitation	300 rpm
T <sub>on</sub> , T <sub>off</sub>	0.001 s, 0.01 s

To prepare the co-electrodeposition bath, the nano sized CeO<sub>2</sub> powder is added to the plating bath and ultrasonicated for 6 h to disperse the nanoparticles. The CeO<sub>2</sub> powder is ball milled for 20 h to obtain a range of the nanoparticles. The CeO<sub>2</sub> concentration is varied from 1 to 30 g/L. The codes for the samples with different CeO<sub>2</sub> concentration are given in Table 2. Steel plate (Merck, electrolytic grade, 99.8%) of 6 cm<sup>2</sup> surface area is used as the cathode and tin metal plate (Merck, electrolytic grade, 99.8%) of approximately 10 cm<sup>2</sup> surface area is used as the anode. The cathode substrate is prepared metallographically and degreased in ultrasonicator for 30 min to remove the dust particles and foreign impurities. Pulse electrodeposition is carried out using a potentiostat/galvanostat Autolab PGSTAT 302N with a 10 A current booster. The electrochemical measurements are performed by Ecochemie software applications.

## 2.2. Microstructural characterization

### 2.2.1. Particle size distribution

The CeO<sub>2</sub> powder particles are analyzed for their particle size by a particle size distribution analyzer (Microtrac–Zetatrac). The measurement technique is that of dynamic light scattering of colloidal particles in suspension. A colloidal suspension of the powder particles is made in Triton X-100 solution. The velocity distribution of the particles suspended is known as function of particle size. Light scattered from each particle is Doppler-shifted by particle motion (Brownian motion). The optical system sends the signal to a photodetector and further analyzed by Microtrac® FLEX Windows Software, using proprietary algorithms, to provide the particle size distribution.

### 2.2.2. X-ray diffraction (XRD)

The monolithic Sn and the composite samples are characterized in a XRD machine (Bruker's D8 Advance) with a vertical goniometer and a Cu target operating at 40 kV and 30 mA that provides X-rays with  $\lambda = 0.154$  nm. The phases formed are identified by comparing the recorded diffraction peaks with the standard ICDD database using X'Pert HighScore software.

### 2.2.3. Scanning electron microscopy (SEM)

Pulse electrodeposited films are analyzed using a scanning electron microscope (Zeiss EVO-40) operating at 20 kV. The SEM is coupled with ultra thin window energy dispersive X-ray spectrometer (EDS), which detects the energy of the characteristic X-rays. This is used to detect the elemental distribution present in the sample.

### 2.2.4. Transmission electron microscopy (TEM)

As deposited films are analyzed using a transmission electron microscope (Phillips FEI Technai G220S-Twin) operating at 200 kV. The samples are prepared by twin jet electro polishing. The twin jet electro polishing (Fishione Model 120) is

**Table 2**  
Sample designations.

Sample codes	Amount of CeO <sub>2</sub> (g/L)
C0	0
C1	1
C2	2
C5	5
C10	10
C15	15
C20	20
C25	25
C30	30

carried out in an electrolyte containing 75% ethanol and 25% phosphoric acid (by volume) at –12 °C and 5 V. The electropolished samples are dried with water followed by alcohol and then stored at room temperature for characterization.

## 2.3. Evaluation of properties

### 2.3.1. Microhardness

Leica VMHT hardness tester (with a tip angle of 136°) is used for the measurement of the microhardness. The corresponding values of Vickers microhardness are calculated as:

$$Hv = 1.854P/d^2 \quad (1)$$

where  $P$  is the applied load in  $kgf$  and  $d$  is the mean length of diagonals in  $\mu m$ . The applied load and loading period are 25  $gf$  and 20 s, respectively. For each sample, microhardness at 10 different points are measured and the arithmetical mean values are reported as the final microhardness.

### 2.3.2. Density

The composites are weighed separately in air ( $W_{air}$ ) and distilled water ( $W_{water}$ ) by high precision electronic balance (Sartorius CPA 225D). The density of the samples is calculated by Archimedes principle based on the following equation:

$$\rho_{sample} = \left( \frac{W_{air}}{W_{air} - W_{water}} \right) * \rho_{water} \quad (2)$$

where  $\rho$  denotes the corresponding density.

### 2.3.3. Surface roughness

The roughness values of the as deposited samples are calculated from the stylus surface profilometer (Veeco Dektak 150 profiler). It consists of a diamond-tipped stylus which takes the measurements electromechanically. The selected programmed scan length used is 2000  $\mu m$  at a scan speed of 66.7  $\mu m/s$ . The stylus is mechanically coupled to the core of a Linear Variable Differential Transformer device. The digital signals from a single scan are stored in computer memory for display and measurement of the data.

### 2.3.4. Wear and friction

Wear and friction tests of the samples are carried out using a standard ball on disk wear tester (DUCOM, TR-208-M1) with a hardened steel ball of 2 mm diameter, and employing different loads (4–10 N) for a total time of 1800 s. The volume loss is obtained using a profilometer (Veeco Dektak 150), and the wear rate is calculated using the formula,

$$\text{wear rate} = [V/NL] \text{ mm}^3/\text{Nm}, \quad (3)$$

where  $V$  is the wear volume loss,  $N$  is the load in Newton, and  $L$  is the sliding distance in m.

### 2.3.5. Resistivity measurements

The resistance  $\frac{V}{I}$  of the as deposited film of Sn and Sn based composites are measured using a four probe setup (Keithley Model 2400) and resistivity is calculated using the formula:

$$\rho = \frac{\pi}{\ln(2)} h \cdot \frac{\Delta V}{I} \quad (4)$$

where  $h$  is the thickness of the film,  $a$  is distance between the two probes,  $V$  is voltage,  $I$  is the current.

## 3. Results and discussions

### 3.1. Synthesis of CeO<sub>2</sub> nanopowders

Fig. 1 shows the particle size distribution of the CeO<sub>2</sub> powders prepared by 0 and 20 h ball milling. It is observed that for 0 h powder, the average particle diameter of the distribution lies around 176 nm, while for 20 h the maximum amount of CeO<sub>2</sub> particles lies in the interval 30–40 nm.

### 3.2. Synthesis of Sn–CeO<sub>2</sub> composite

#### 3.2.1. XRD

Fig. 2 shows the XRD patterns of pure monolithic Sn and Sn–CeO<sub>2</sub> nanocomposite coatings synthesized by the process of pulse electrodeposition. The XRD pattern of Sn–CeO<sub>2</sub> nanocomposite

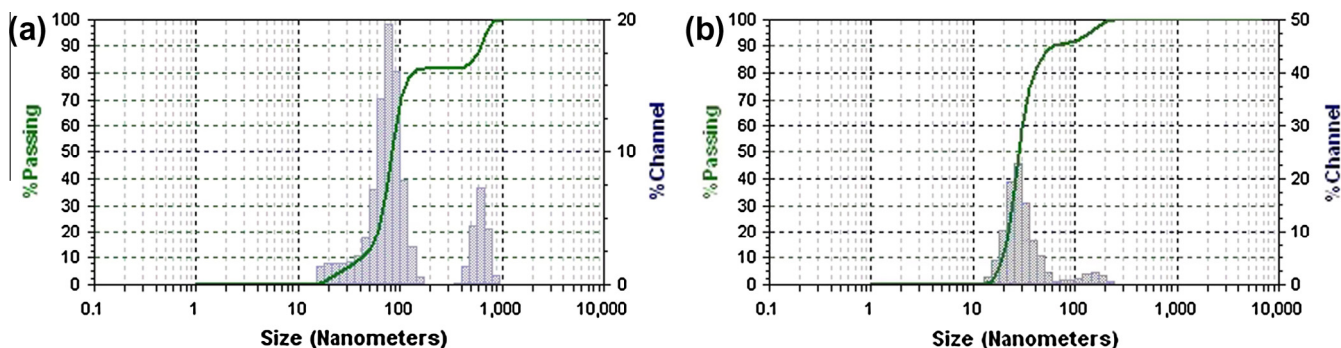


Fig. 1. Particle size distribution of the CeO<sub>2</sub> powder ball milled for (a) 0 and (b) 20 h.

shows the presence of (111) CeO<sub>2</sub> peak along with the peaks from Sn matrix. This confirms that the co-electrodeposition of CeO<sub>2</sub> particles in the matrix is successfully achieved.

### 3.2.2. SEM

The surface morphology of monolithic Sn and Sn–CeO<sub>2</sub> composites is shown in Fig. 3. The microstructure of the deposits consists of pyramid shaped grain clusters. It is observed that an increase in concentration of CeO<sub>2</sub> nanoparticles in the electrolyte upto 15 g/L leads to fine grained and compact deposits. The particle incorporation increases the number of nucleation sites and also limits the grain growth of the matrix resulting in a fine grained microstructure [16]. In the present case, the grain size of Sn is reduced with an addition of CeO<sub>2</sub> but still it lies in the micrometer range. The best morphology of the Sn–CeO<sub>2</sub> composite is obtained when it is deposited from the electrolyte containing 15 g/L CeO<sub>2</sub>. At this concentration of CeO<sub>2</sub> in electrolyte, the matrix consists of monodispersed CeO<sub>2</sub> as shown in Figs. 3f and j. The formation of cracks and pores can be seen in the composites when they are deposited from electrolyte containing more than 15 g/L CeO<sub>2</sub> as shown in Fig. 3g–i. Fig. 3k shows the presence of agglomerated CeO<sub>2</sub> particles in the composite matrix. This is correlated to the fact that due to a high concentration of CeO<sub>2</sub> in electrolyte, their interparticle distance decreases and the particles come closer to form agglomerates. As a result, they have difficulties in reaching towards the cathode and hence an agglomerated/non uniform deposit is observed.

SEM observation of the Sn matrix composite (C15) shows the maximum dispersion of the fine particles (CeO<sub>2</sub>) in the matrix.

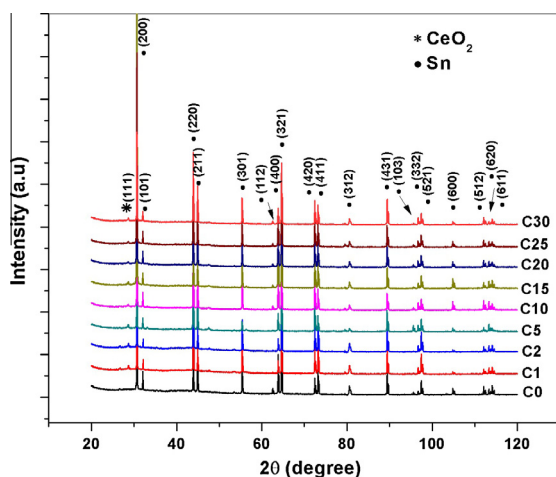


Fig. 2. XRD patterns of the pure Sn and Sn–CeO<sub>2</sub> composite prepared from the electrolytic bath containing different concentration of CeO<sub>2</sub>.

The amount of the co-electrodeposited CeO<sub>2</sub> in the Sn matrix is analyzed by EDS and is plotted in Fig. 4. It is seen from Fig. 4 that as the concentration of CeO<sub>2</sub> in the electrolyte increases, the amount of co-electrodeposited CeO<sub>2</sub> in the Sn matrix also increases upto C15 and then a decrease is observed. Initially as the particle concentration is less, the mobility of the particles in the electrolyte is high. This results in uniformly codeposited CeO<sub>2</sub> in the Sn matrix. But as the particle concentration increases beyond 15 g/L, their mobility decreases and the particles are attracted under weak Van der Waals interaction to form CeO<sub>2</sub> agglomerates which are difficult to get codeposited and whatever is deposited is in agglomerated form. Thus, a drop in CeO<sub>2</sub> content in matrix is observed. This results in the deposits with agglomerated CeO<sub>2</sub> particles, and formation of cracks (sample C20), and big pores (C25 and C30), as shown in Fig. 3.

### 3.2.3. TEM

Fig. 5 shows (a) TEM bright field and (b) dark field images of the as deposited nanocomposite coating. The CeO<sub>2</sub> nano particles are clearly observed in the dark field image and are about ~20 nm in size. The selected area diffraction (SAD) pattern of the coating (Fig. 5c) shows the presence of ring pattern of CeO<sub>2</sub> superimposed with the spot pattern obtained from the Sn matrix. This further confirms the co-electrodeposition of CeO<sub>2</sub> nanoparticles in the Sn matrix.

## 3.3. Evaluation of properties

### 3.3.1. Microhardness

In order to investigate the mechanical performance of the coatings, the Vicker's microhardness is measured, Fig. 6. The microhardness values of the composite solders show a continuous increasing trend with the increase in the amount of CeO<sub>2</sub> particles upto 15 g/L CeO<sub>2</sub> in electrolyte. There are basically a number of causes for this enhancement in the microhardness of composite samples, such as (a) the higher hardness of CeO<sub>2</sub> as compared to the matrix (b) the dispersion hardening effect of CeO<sub>2</sub> particles in the Sn matrix, and (c) grain refinement of the matrix since CeO<sub>2</sub> provides more nucleation centers during electrodeposition and also restricts the grain growth [17].

It is also observed that the hardness of the composites start to decrease when they are deposited from the electrolyte containing more than 15 g/L CeO<sub>2</sub>. The microhardness of C20, C25 and C30 is lower than C15. It is already mentioned that in these samples, the total amount of CeO<sub>2</sub> particles incorporated is quite less compared to the sample C15. Moreover, the CeO<sub>2</sub> is present in the agglomerated form, as already observed from the SEM micrographs (Fig. 3). These factors lead to a weakening in the described strengthening mechanisms and thus lowering the composite microhardness.

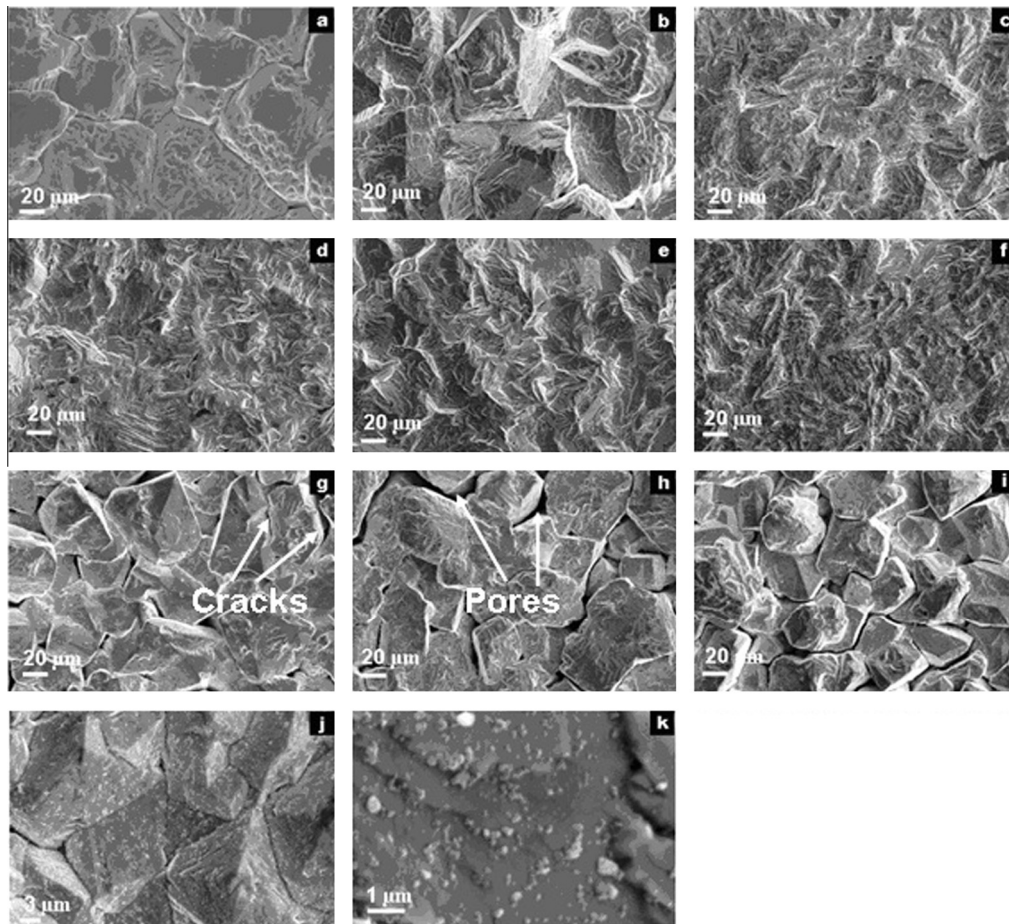


Fig. 3. Surface morphology of the pure Sn and Sn-CeO<sub>2</sub> nanocomposites (a) C0, (b) C1, (c) C2, (d) C5, (e) C10, (f) C15, (g) C20, (h) C25 and (i) C30, (j) high magnification micrograph of C15 showing maximum distribution of CeO<sub>2</sub>, and (k) magnified view of (i) showing agglomeration in sample C30.

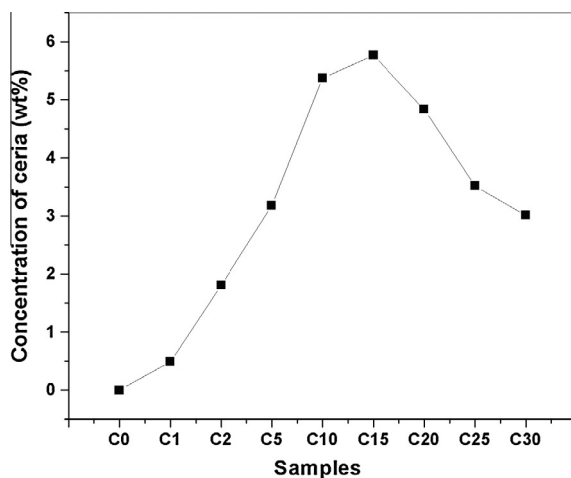


Fig. 4. Amount of codeposited CeO<sub>2</sub> in the nanocomposite coatings.

### 3.3.2. Density

The density of the samples is calculated by Archimedes law and reported in Fig. 7. It is observed that the density of sample C0 is  $\sim 7.27 \text{ g/cm}^3$ . The reported values of density at room temperature for Sn and CeO<sub>2</sub> are 7.28 and 7.21  $\text{g/cm}^3$ , respectively [18,19]. The measured density of the developed composite samples is lower as compared to the monolithic samples. With increasing concentration of reinforcements the density of all the investigated

composite solders is found to decrease. The apparent density decrease is not due to the incorporation of CeO<sub>2</sub>, since CeO<sub>2</sub> has very similar density to pure Sn. This decrease is due to the increase of porosities in the coatings with an incorporation of CeO<sub>2</sub> in the coatings. The observed density is minimum for the composite when it is prepared from 30 g/L CeO<sub>2</sub> in electrolyte, (i.e., 6.695  $\text{g/cm}^3$  for C30) which has not only a higher amount of pores, but also cracks form in the coating. It has been reported in the literature that build up of porosities and cracks in the composite sample due to the addition of reinforcements can be detrimental to the mechanical properties [5,20,21]. Although the density is lesser for the composites developed from more than 15 g/L CeO<sub>2</sub> in electrolyte, yet in view of the poor mechanical properties they are not suggested for light weight application.

### 3.3.3. Wear and friction behavior

**3.3.3.1. Surface roughness and microhardness.** For the wear and friction study, the Sn-CeO<sub>2</sub> coating with the maximum hardness (C15) is taken under investigation and compared with the pure Sn. The surface roughness values have been measured for the wear property evaluation and tabulated along with the microhardness values as shown in Table 3. These two parameters play an important role in determining the wear resistance of a material [22]. From Table 3, it can be seen that the roughness value of the composite is higher as compared to the monolithic sample. The presence of reinforcement phases on the surface will act as a surface projection and thus increases the roughness.

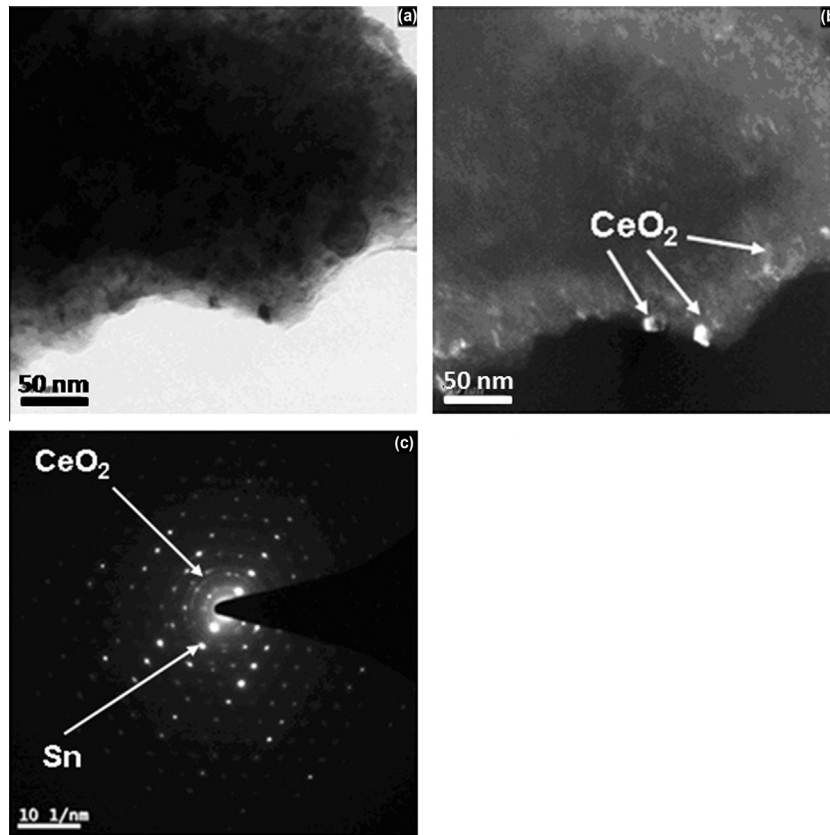


Fig. 5. TEM micrographs of Sn–CeO<sub>2</sub> nanocomposite showing (a) BF image, (b) DF image and (c) SAD pattern of (a).

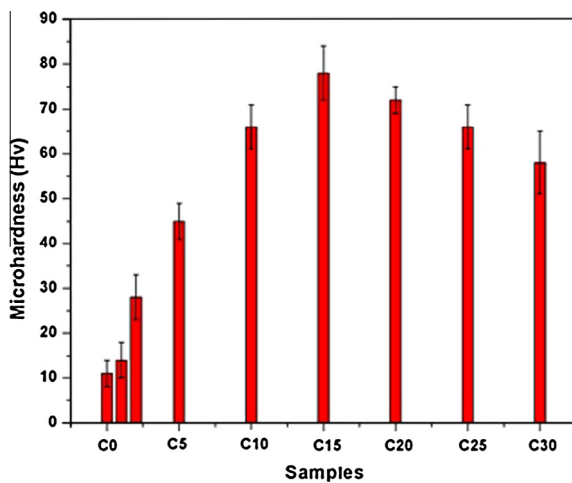


Fig. 6. Microhardness of pure Sn and Sn–CeO<sub>2</sub> composite coatings.

**3.3.3.2. Wear rate.** The wear rates of the selected samples are shown in Fig. 8a. It is observed that pure Sn is having a higher wear rate compared to that of Sn–CeO<sub>2</sub>. The result is in good agreement with the Archard's relation [23], which states that harder samples possess higher wear resistance. The incorporation of CeO<sub>2</sub> nanoparticles improves the wear resistance of the composite solders due to the higher hardness and strength brought about by dispersion of the CeO<sub>2</sub> nanoparticles in the matrix. An increase in load, from 4 to 10 N causes an increase in wear rate for Sn and its composite as expected.

**3.3.3.3. Coefficient of friction (COF).** The average values of COF for different samples as a function of loads are plotted in Fig. 8b. The

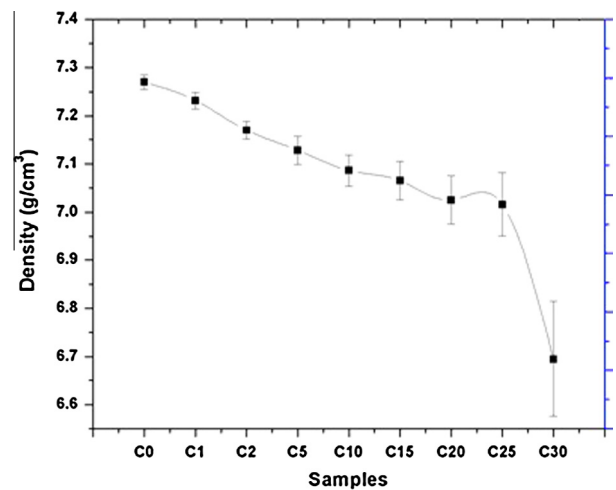


Fig. 7. Density as a function of CeO<sub>2</sub> concentration for different composites.

Table 3

Roughness and microhardness values of the samples under investigation for wear test.

Samples	Roughness (μm)	Microhardness (Hv)
C0	4.04	11
C15	9.4	78

measured roughness for C0 and C15 are 4.04 and 9.4 μm, respectively (Table 3). It is observed that the COF value of the composite samples is higher than that of the monolithic samples. It has been argued in the literature that wear rate depends on the value of

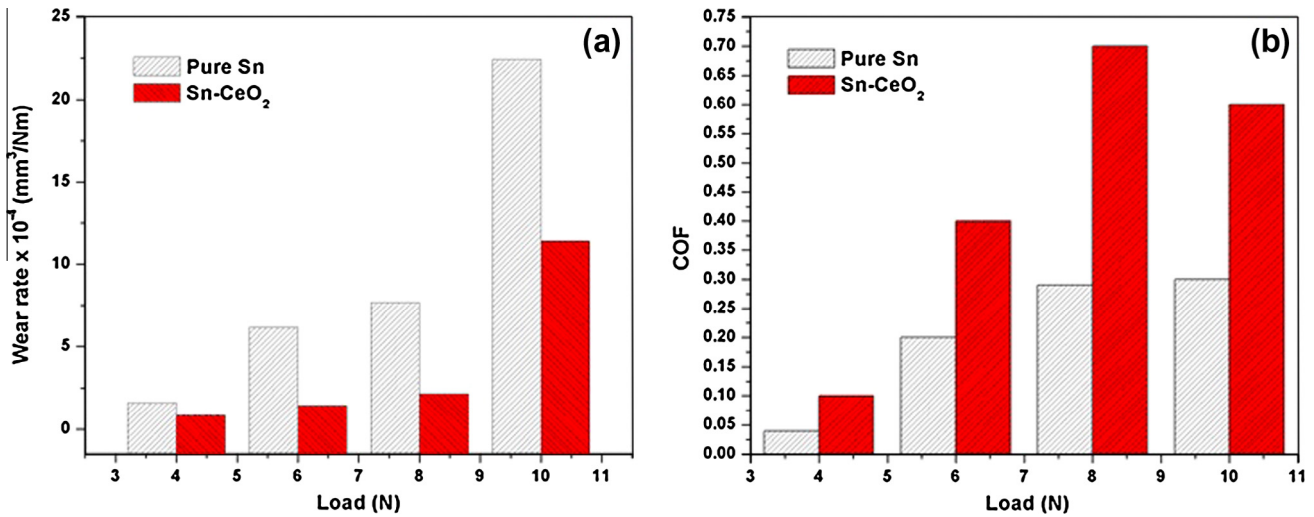


Fig. 8. (a) Wear rate and (b) COF of the pure Sn (C0) and Sn-CeO<sub>2</sub> composite (C15).

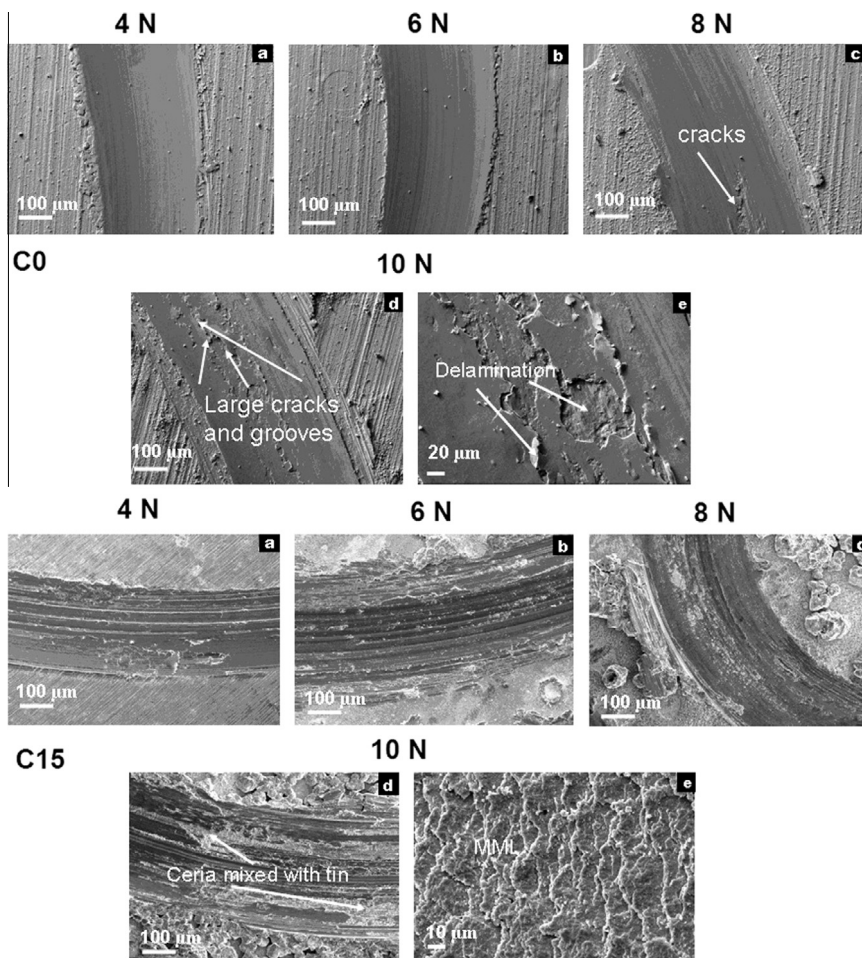


Fig. 9. SEM micrographs showing the wear track morphology of C0 and C15 at different loads, (a) 4, (b) 6, (c) 8, (d) 10 N and (e) high magnification image of (d).

microhardness but COF depends on the roughness values of the surface [24]. As load increases from 4 to 8 N, the increase in COF is observed for the all the samples. In the case of the C15 composite sample, the COF increases at a higher rate due to its higher surface roughness.

It is also noticed that for C15 there is a slight drop in the COF as the load exceeds 8 N. This may be due to the fact that in case of C15, the soft Sn matrix and hard CeO<sub>2</sub> particles which come out from the coating may get mixed in due course of sliding and form mechanically mixed layer (MML). This type of MML formed at the

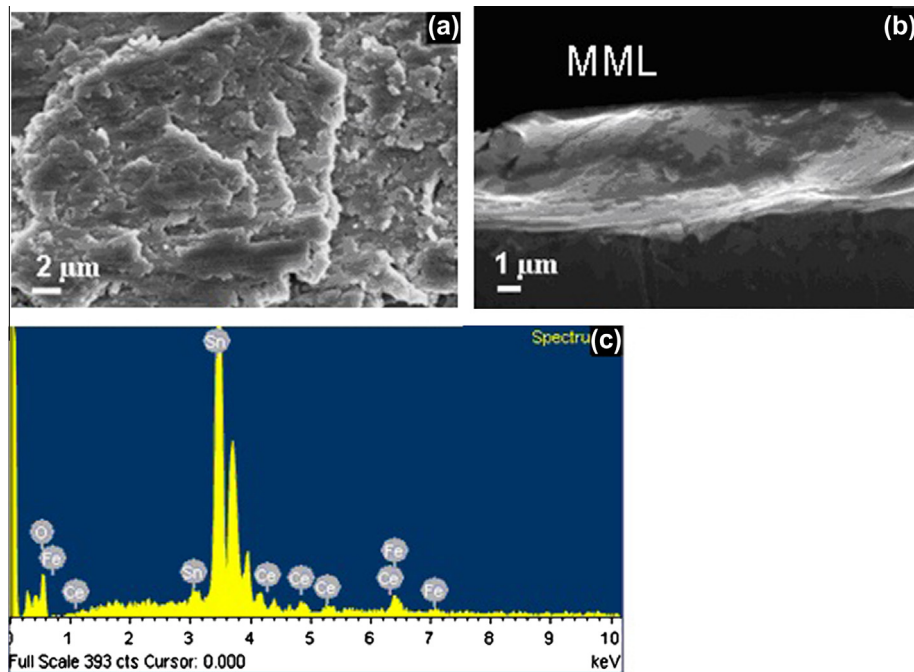


Fig. 10. (a) High magnification SEM image of the wear track in C15 at 10 N, (b) cross sectional view of (a), and (c) the EDS spectrum.

wear surface will create a smoothing effect on the surface and decrease the friction.

**3.3.3.4. Worn surface morphology.** SEM micrographs of wear tracks of samples C0 and C15 at different loads are shown in Fig. 9. It is observed from Fig. 9 that in case of C0, the width of tracks increases with an increase in load. As the load increases from 4 to 6 N, the width of the wear track increases gradually and the wear track appears smooth due to the soft and ductile nature of Sn. With further increase in load to 8 N, cracks nucleate on the subsurface, as shown in Fig. 9c. An excessive load of 10 N results in propagation of the nucleated cracks and ultimately chipping out of the tracks. The chipped regions get detached from the track which finally leads to the failure, as shown in Fig. 9d and e. This type of loose sheet or flake like wear debris formation suggests the failure of coating by delamination wear [25].

In case of C15, the width of the wear tracks is narrower than that of the same in C0. As the load is increased from 4 to 8 N, the wear track width increases but slowly as the CeO<sub>2</sub> particles present on the surface obstruct the plastic deformation of the matrix. When the load exceeds 8 N, it appears that loose CeO<sub>2</sub> particles are getting mixed with the matrix in due course of sliding (CeO<sub>2</sub> particles are shown in white color), as shown in Fig. 9d and e. This observation also supports the fact that the COF of sample C15 decreases at 10 N due to the formation of MML, as discussed in previous Section 3.3.3.3.

To further confirm this phenomenon, a close examination of the plane and cross sectional view of the wear tracks is done in SEM (Fig. 10a and b). The EDS analysis is also performed at the central region of wear track as shown in Fig. 10c. The plane view SEM image shows that there is formation of a layer by layer structure in the wear track. The cross sectional SEM micrograph confirms the wavy pattern of this structure that is acquired during the mixing process.

The EDS spectrum shows the presence of Sn, CeO<sub>2</sub>, and a little amount of Fe which is likely to come from the steel ball of the wear testing machine. The wear debris generated during sliding may go outside the wear track or be trapped by the two sliding surfaces

and eventually undergo mechanical mixing process. The presence of Fe implies the transfer of counterface materials to the worn surface. The oxygen peak suggests that oxidative wear is also playing a role. Since this type of surface layer contains materials from both the counter surfaces, it is called mechanically mixed layer [26,27].

### 3.3.4. Electrical resistivity

The electrical resistivity of the composites, shown in Fig. 11, always increases with CeO<sub>2</sub> concentration. It is noteworthy that the increase in magnitude is very slow upto samples deposited from 15 g/L CeO<sub>2</sub> in electrolyte; while beyond this concentration there is a marked increase in the resistivity. This can be better explained considering Matthiessen's rule [26]. It states that the total resistivity of a material is the sum of three components: (i) foreign impurities ( $\rho_i$ ), (ii) thermal agitations of metal ions of lattice ( $\rho_t$ ), and (iii) presence of imperfections in the crystal, e.g., pores, deformation ( $\rho_d$ ), etc. Thus, total resistivity can be given as,

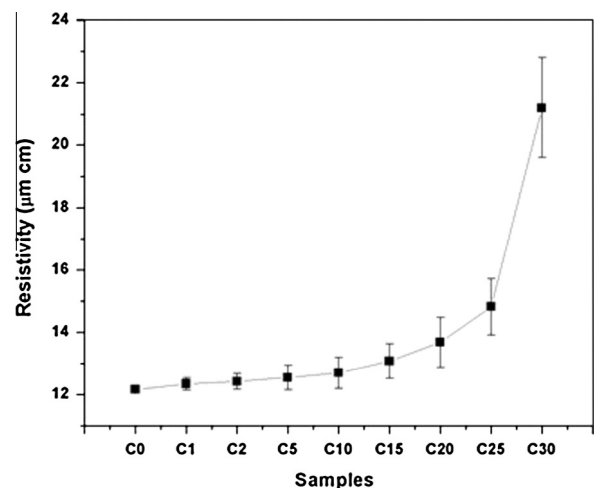


Fig. 11. Electrical resistivity of the pure Sn and Sn-CeO<sub>2</sub> composites.

$$\rho = (\rho_i) + (\rho_t) + (\rho_d) \quad (5)$$

For composite solders, the total resistivity values are thus expected to increase due to the larger contributions of  $\rho_i$  and  $\rho_d$  when compared to that of monolithic solder samples. The value of  $\rho_d$  depends on several factors such as volume fraction of the pores ( $V_p$ ), plastic zone ( $V_{pz}$ ) and reinforcement ( $V_r$ ). The effective volume fraction of scattering centers, ( $V_T$ ), can now be represented as follows:

$$V_T = V_{pz} + V_r + V_p \quad (6)$$

For a particulate reinforcement the volume fraction of the deformation region surrounding the reinforcement,  $V_{pz}$ , is expressed by

$$V_{pz} = (\alpha^3 - 1)V_r \quad (7)$$

where  $\alpha$  is the ratio of the size of the heterogeneous nucleation zone to that of the reinforcement [28].

Rearranging (6) and (7),

$$V_T = (\alpha^3 - 1)V_r + V_r + V_p = \alpha^3 V_r + V_p \quad (8)$$

The value of  $\alpha$  depends on the type of matrix and also the size, shape, and type of the reinforcement, but not on its volume fraction. Thus, according to Eq. (8) the effective volume fraction depends on the volume fraction of reinforcement and pores.

It is noted from Fig. 11 that the resistivity increase is very slow for the samples deposited from the electrolyte containing upto 15 g/L CeO<sub>2</sub> (i.e., C15). For example, from C0 to C15 there is a slow increase in resistivity from 12.16 to 13.08  $\mu\Omega$  cm. This may be due to the fact that the porosity contribution,  $V_p$ , is not significant to cause much disturbance in electron path. Thus omitting the porosity ( $V_p$ ) term in Eq. (8), resistivity will increase with only the volume fraction of the CeO<sub>2</sub> nanoparticles ( $V_r$ ). Hence, the total resistivity increases but the amount of increase is not so high. However, the resistivity increases at a considerable rate for those samples which are deposited from electrolytes containing more than 15 g/L CeO<sub>2</sub> and especially, it is very high for C30. This can be expected since the resistivity is also getting affected by the presence of the significant amount of porosities and cracks in these samples. These porosities and cracks act as additional scattering centers to the path of the electron motion and increase resistivity. The electrical resistivity of Sn–CeO<sub>2</sub> based nanocomposite solders measured are quite comparable with other composites like Sn–0.7Cu/Al<sub>2</sub>O<sub>3</sub>, Sn–Ag/SnO<sub>2</sub>, Sn–Ag/Y<sub>2</sub>O<sub>3</sub>, etc. [29].

#### 4. Conclusions

1. Sn–CeO<sub>2</sub> composite solder coating has been processed successfully from aqueous citrate bath using pulse co-electrodeposition technique. The incorporation of CeO<sub>2</sub> particles in the matrix increases with an increasing CeO<sub>2</sub> concentration in the electrolyte upto 15 g/L, and then decreases due to the agglomeration of CeO<sub>2</sub> particles in the bath. The best morphology of the composites is realized at 15 g/L CeO<sub>2</sub> in the electrolytic solution that gives 5.8 wt% CeO<sub>2</sub> in Sn matrix.
2. The incorporation of CeO<sub>2</sub> in the Sn matrix results in a tremendous increase in the microhardness of the composite solder over the unreinforced monolithic material.
3. The density of Sn–CeO<sub>2</sub> composites decreases with an increase in concentration of CeO<sub>2</sub> in the electrolyte due to the formation of porosities in the composites. The observed density is

minimum for the composite when it is prepared from an electrolyte containing 30 g/L CeO<sub>2</sub>. A very low density of Sn–CeO<sub>2</sub> composite when deposited from the electrolyte containing 30 g/L CeO<sub>2</sub> is due to the formation of both porosities and cracks.

4. The addition of reinforcement in the Sn matrix also improves the wear resistance, which ultimately increases the coating life for application. The wear resistance of the composite coatings is better than that of the monolithic material and it is associated with an enhancement in the microhardness of the composite.
5. At all loads studied here, monolithic material exhibits the lower coefficient of friction compared to the composite coating due to the higher roughness values of composite. The coefficient of friction is found to increase as loads are increased from 4 to 10 N for all the samples, except for Sn–CeO<sub>2</sub> composite. This particular composite shows a reduction in coefficient of friction at a load of 10 N and this is attributed to the formation of mechanically mixed layer in this system.
6. There is a rise in the resistivity of the composite matrix compared to the monolithic material. However, the resistivity of the composites falls within the usable limits as reported for other Sn based composites, used for electrical contact applications.

#### References

- [1] C. Harper, *Electronic Materials and Processes Handbook*, Mc GrawHill, New York, 2004.
- [2] K. Suganuma, *Curr. Opin. Solid State. Mater.* 5 (2001) 55–64.
- [3] M. Abtew, G. Selvaduray, *Mater. Sci. Eng. R* 27 (2000) 95–141.
- [4] F. Guo, *J. Mater. Sci.: Mater. Electron.* 18 (2007) 129–145.
- [5] X.L. Zhong, M. Gupta, *J. Phys. D: Appl. Phys.* 41 (2008) 095403.
- [6] P. Babaghorbani, S.M.L. Nai, M. Gupta, *J. Mater. Sci.: Mater. Electron.* 20 (2009) 571–576.
- [7] A. Lee, K.N. Subramanian, J. Lee, Development of nanocomposite lead-free electronic solders, in: *Proc. International Symposium on Advanced Packaging Materials: Processes, Properties and Interfaces*, Irvine, California, USA, IEEE, 2005, pp. 276–281.
- [8] S. Chen, L. Zhang, J. Liu, Y. Gao, Q. Zhai, *Mater. Trans.* 51 (2010) 1720–1726.
- [9] P. Liu, P. Yao, J. Liu, J. Electron. Mater. 37 (2008) 874–879.
- [10] J. Wei, S.M.L. Nai, C.K. Wong, M. Gupta, *Simtech. Tech. Reports* 6 (2005) 29–32.
- [11] M.A.A. Mohd Salleh, A.M. Mustafa Al Bakri, H. Kamarudin, M. Bnhussain, M.H. Zan@Hazizi, F. Somidin, *Phys. Procedia.* 22 (2011) 299–304.
- [12] J. Shen, Y.C. Liu, Y.J. Han, Y.M. Tian, H.X. Gao, *J. Electron. Mater.* 35 (2006) 1672–1679.
- [13] X. Liu, M. Huang, C.M.L. Wu, L. Wang, *J. Mater. Sci.: Mater. Electron.* 21 (2010) 1046–1054.
- [14] E.K. Choi, K.Y. Lee, T.S. Oh, *J. Phys. Chem. Solids* 69 (2008) 1403–1406.
- [15] S.T. Aruna, C.N. Bindu, V.E. Selvi, V.K. William Grips, K.S. Rajam, *Surf. Coat. Technol.* 200 (2006) 6871–6880.
- [16] M. Venu, *Synthesis and Characterization of Ceria Reinforced Copper Matrix Nanocomposite Coatings*, PhD Thesis, IIT Kharagpur, India, 2011.
- [17] M. Venu, S. Bhattacharya, K. Das, S. Das, *Surf. Coat. Technol.* 205 (2010) 801–805.
- [18] J.Y. Song, J. Yu, T.Y. Lee, *Scripta Mater.* 51 (2004) 167–170.
- [19] Y. Kobayashi, Y. Fujiwara, *J. Alloys Comp.* 408–412 (2006) 1157–1160.
- [20] H. Mavoori, S. Jin, *J. Electron. Mater.* 27 (1998) 1216–1222.
- [21] S.M.L. Nai, J. Wei, M. Gupta, Influence of ceramic reinforcements on the wettability and mechanical properties of novel lead-free solder composites, *Thin Solid Films* 504 (2006) 401–404.
- [22] R. Sen, *Synthesis and Characterization of Pulse Electrodeposited Ni–CeO<sub>2</sub> Nanocomposite Coatings*, PhD Thesis, IIT Kharagpur, India, 2011.
- [23] J.F. Archard, *J. Appl. Phys.* 24 (1953) 981–988.
- [24] A. Iwabuchi, H. Kubosawa, K. Hori, *Wear* 139 (1990) 319–333.
- [25] Y.W. Park, T.S.N. Sankara Narayanan, K.Y. Lee, *Tribol. Int.* 40 (2007) 548–559.
- [26] Y. Zhan, G. Zhang, Y. Zhuang, *Mater. Trans.* 45 (2004) 2332–2338.
- [27] A. Urena, J. Rams, M. Campo, M. Sanchez, *Wear* 266 (2009) 1128–1136.
- [28] S.Y. Chang, C.F. Chen, S.J. Lin, T.Z. Kattamis, *Acta Mater.* 51 (2003) 6191–6302.
- [29] P. Babaghorbani, S.M.L. Nai, M. Gupta, *J. Alloys. Comp.* 478 (2009) 458–461.